Improvement of the spatial resolution of the MicroPET R4 scanner by wobbling the bed

Joon Young Suk[a)]
Brain Research Centre, University of British Columbia, Vancouver V6T 2B5, Canada and McConnell Brain Imaging Centre, Montreal Neurological Institute, Montreal H3A 2B4, Canada

Christopher J. Thompson
McConnell Brain Imaging Centre, Montreal Neurological Institute, Montreal H3A 2B4, Canada

Aleks Labuda
Department of Physics, McGill University, Montreal H3A 2T8, Canada

Andrew L. Goertzen
McConnell Brain Imaging Centre, Montreal Neurological Institute, Montreal H3A 2B4, Canada and Department of Radiology, University of Manitoba, Winnipeg R3E 3P4, Canada

(Received 30 June 2007; revised 17 January 2008; accepted for publication 18 January 2008; published 7 March 2008)

The MicroPET R4 scanner was designed for imaging small rodents such as mice and rats. In many cases the spatial resolution of this system is not sufficient for resolving structures of interest. In order to improve the spatial resolution of the MicroPET R4 through improved spatial sampling, the authors have implemented a variable radius eccentric motion, commonly referred to as wobbling, which is applied to the animal bed during scanning. The wobble motion is incorporated into the sinograms using modified histogramming software, capable of reading the bed wobble position from the list-mode data. The histogramming software corrects the data for the dwell time, apparent crystal location, and crystal-pair efficiency and applies a resolution matching filter. The data acquisition, reconstruction, and image display programs provided from the manufacturer required no modifications. For all studies a wobble period of 8 s was used. The optimal wobble radius was found to be 1.50 mm. The wobbled bed acquisition technique was tested by scanning a resolution phantom and a rat. Images from both studies acquired when using the wobble motion showed an improved spatial resolution when compared with comparable images acquired without the wobble motion. The bed wobbling mechanism can be added to any MicroPET system without major changes and without compromising any imaging modes. Implementing the wobble mechanism may represent a cost-effective method to upgrade the spatial resolution of a MicroPET when compared to the purchase of a newer generation system. © *2008 American Association of Physicists in Medicine*. [DOI: 10.1118/1.2868760]

Key words: positron emission tomography, spatial resolution, wobble mechanism, MicroPET

I. INTRODUCTION

The MicroPET R4 scanner (Siemens Preclinical Solutions, Knoxville, TN) is a dedicated animal positron emission tomography (PET) scanner designed for studies of small animals such as mice and rats. The spatial resolution of the MicroPET R4 was previously reported by Knoess *et al.*[1] as 1.85 mm full width at half maximum (FWHM) in the axial direction and 1.66 mm FWHM in the transaxial direction at the center of the field of view (CFOV) when measured with a 1 mm diameter ^{22}Na point source. While the resolution degrades with increasing radial offset, it is less than 2.5 mm FWHM in all three (axial, radial, and tangential) directions within the 20 mm inner radius of the FOV.

Measured spatial resolution in PET is limited by several factors, such as positron range (pr), source size (ss), scanner ring diameter (ds) leading to noncolinearity, crystal width (cw), and block effect (be). An empirical equation to describe the spatial resolution of a PET scanner was proposed by Derenzo and Moses,[2]

$$\mathrm{SR} = k\sqrt{(\mathrm{pr}+\mathrm{ss})^2 + (0.0022\cdot \mathrm{ds})^2 + \left(\frac{\mathrm{cw}}{2}\right)^2 + \mathrm{be}^2}, \qquad (1)$$

where k is a scaling factor for the image reconstruction algorithm. Equation (1) shows the spatial resolution, (SR), near the CFOV of a PET scanner with a ring diameter ds and crystal width cw. When examining methods to improve the spatial resolution in PET, the positron range represents a fixed minimum resolution that could be achieved. The second term, due to the noncollinearity of the 511 keV annihilation photons, is a function of the system ring diameter. This term is much smaller in dedicated animal scanners with small ring diameters as compared to those used for human whole body imaging. The block effect, be, is an image blur-

ring factor which is introduced by using a block detector design.[3] Though the term block effect had been introduced in 1993, the effect was not fully investigated as a cause of spatial resolution degradation until 10 years later. In the work of Moses *et al.*[2] and Derenzo,[3] it was estimated that the use of light sharing PET block detectors adds a block effect component of 2.3 mm.

From a simplistic perspective, the easiest way to improve the spatial resolution of a PET system is by decreasing crystal width cw. There is already a second generation commercial MicroPET, named the "Focus 120," whose spatial resolution is improved from 2.32 to 1.69 mm at 5.0 mm radial distance from the CFOV in comparison to the MicroPET R4 scanner.[4] The Focus 120 system has more than twice the number of LSO crystals as the R4 scanner, even though it has a similar ring diameter and axial FOV. This increase in crystal number is due to the crystal size being reduced from 2.1 mm in the R4 to 1.5 mm in the Focus 120. While the F120 scanner has improved spatial resolution through the use of smaller crystals, it costs significantly more.

In 2005, Tomic *et al.* reported that the block effect could not be fully explained simply by the light sharing between crystals in a block.[5] They showed that the intrinsic block effects for various PET scanners, including the MicroPET R4 scanner, were much smaller than the 2.3 mm value which had been observed by Lecomte,[6] and proposed and observed by Moses.[2,3] Thompson *et al.*[7] demonstrated that to fully describe the block effect, the effects of spatial "undersampling" have to be considered. This article showed that it was possible to reduce the image blurring due to the block detector by increasing the spatial sampling without decreasing the crystal width.

Before the introduction of the block detector, the technique of wobbling was used to increase spatial sampling since the width of crystals in early PET scanners was much greater than those currently used. The PETT VI scanner was the first PET scanner to use the wobbling motion of the detector array to improve the sampling in 1982 (Ref. 8) and in 1989 a substantial improvement was made.[9] The Scanditronix 2048B brain PET scanner employed both block detectors and a detector wobble motion.[10] We hypothesized that one could get a similar improvement of the spatial sampling by wobbling the bed instead of wobbling the whole detector ring. For small animal PET scanners this would be a more effective way of implementing a wobbling motion as the animal bed is a simple structure and is much lighter than the detector system. In 2000, Chatziioannou *et al.* increased the spatial sampling of the original MicroPET by moving the bed in a discontinuous manner and collecting data at several points.[11] They demonstrated significant improvement in spatial resolution in both phantom and animal imaging. Previous data with discontinuous detector movement (unpublished data obtained with Positome II in 1980) and continuous wobbling[9,12] demonstrated the superiority of continuous wobbling. With continuous motion, the sampling is uniform in all projections whereas the data sets from different "steps" of the "step and shoot" have varying sampling density after interleaving to form a single projection. Furthermore, with continuous wobbling, there is only one data set, so no interleaving is required. These differences make continuous wobbling better than discontinuous movement to improve the spatial resolution of the scanners.

In this article, we describe in detail the bed wobble mechanism as well as the new histogramming software which incorporates all the corrections required to reconstruct quantifiable images with higher spatial resolution. The optimal wobble radius and peak-to-valley ratio are discussed. Images of a spatial resolution phantom and a rat demonstrate the improvements in resolution obtained during wobbled scans.

II. MATERIALS AND METHODS

II.A. Wobble mechanism

In order to perform the wobble motion of the animal bed during the data acquisition, we built a mechanical system that supports the animal bed of MicroPET R4 scanner. The support for the wobble mechanism has been designed to replace the top plate of the bed support with one that provides the support for eccentric bearings and the drive for the wobble motion. Addition of the wobbling mechanism did not alter the range of motion or functionality of the bed.

Figure 1(a) shows a design drawing of the side view of the wobble mechanism. A small low voltage electric motor drives two axles via a timing belt. These axles have rotating disks at each end. A smaller disk is attached to each disk and the center of the two disks is misaligned as shown in the inset photo of Fig. 1(a). The centers of the smaller disks have bearings and short axles to which the new bed support is attached with screws that pass through their centers. The offset distance between the two wheels becomes the radius of the wobble circle on which all parts of the bed support, bed, and its contents are constrained and will move when the motor turns. The wobble radius can be adjusted from 0.25 to 1.75 mm in steps of 0.25 mm. This allowed us to perform experiments with various wobble radii in order to optimize the sampling. Figure 1(b) shows how one produces the desired wobble motion with two eccentric wheels. Eight pairs of screw holes surround the center of the bigger wheel and the offset distance between the center of the wheel and the center of each pair of holes varies from 0.25 to 1.75 mm. These offsets are equivalent to the wobble radii. The smaller wheel is fixed on the bigger wheel by pins screwed into a pair of holes among the eight pairs through holes on itself. The finished wobble mechanism, which is installed underneath an animal bed of MicroPET R4 scanner, is shown in Fig. 2.

The wobble controller (Fig. 2) is located at the side of the bed support. It starts and stops the wobbling motion and adjusts the speed. The system starts wobbling as soon as the start button is pressed. When the stop button is pressed, the motion stops at the origin of the wobble motion which is detected by a microswitch. This ensures that the wobble system starts and stops in the same position for every scan. This

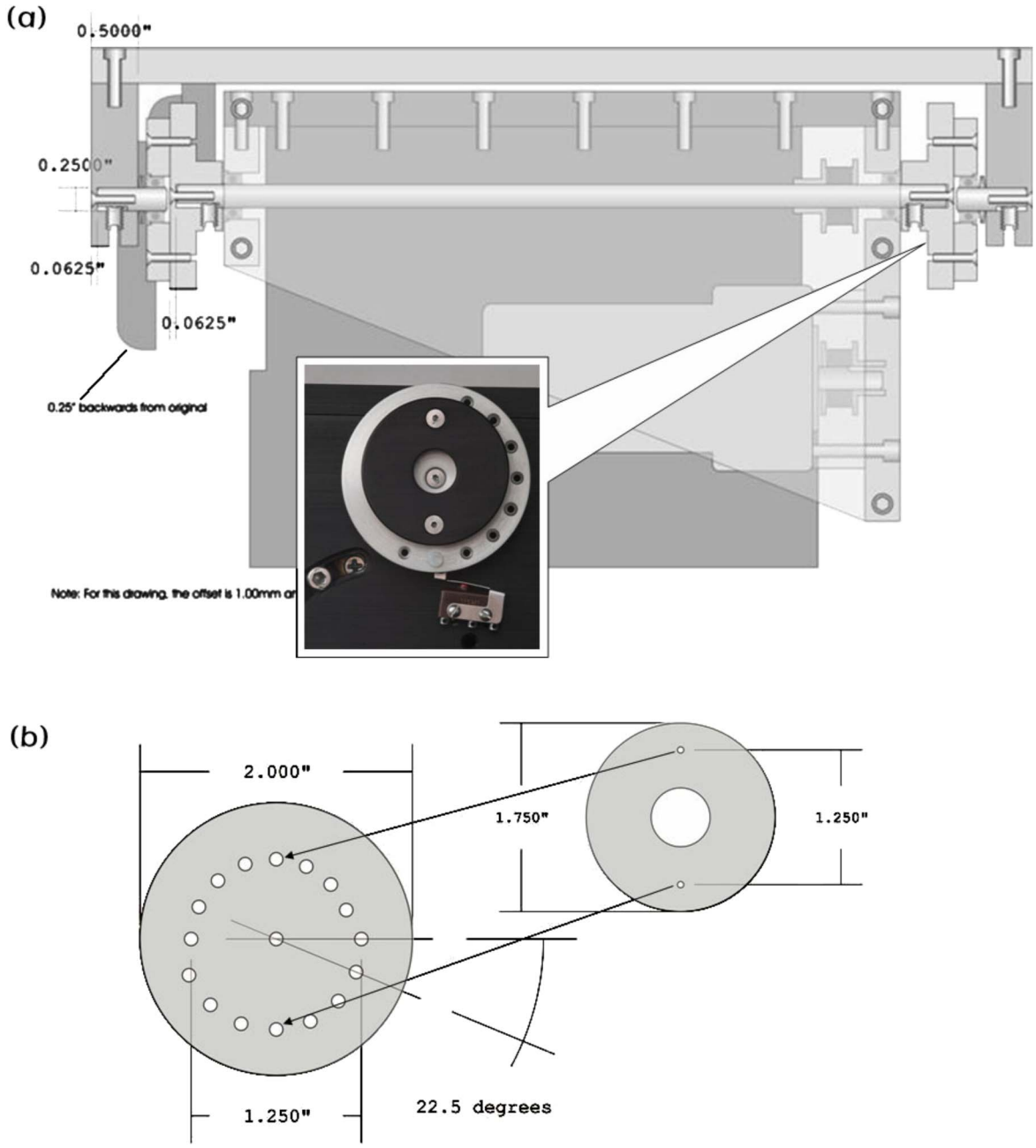

FIG. 1. (a) Schematic of wobble mechanism. (b) A detail drawing of two eccentric wheels.

microswitch also generates a gating signal to the MicroPET system. When the microswitch is depressed, a multivibrator generates a pulse train which is fed to one of the gating inputs and thus causes a "gate event" to be entered into the list-mode data from the scanner.[13]

II.B. Histogramming program

A new histogramming program was required to take into account the wobble correction since the program supplied with the scanner cannot handle the wobble data. The wobble motion is used to increase the spatial sampling density in the sinograms. By experimenting with the input parameters to the MicroPET reconstruction program we found that it could accept an increase in sampling density by a factor of either 3 or 5. Therefore, each wobble cycle can be divided into three or five bins. Since the animal bed is continuously wobbled while the object is being scanned, several corrections must be considered with proper weighting factors. First of all, the location of the bed during wobble cycle is required to estimate the wobble offset. It is possible to estimate the current angle of the animal bed by using successive gate signals from the microswitch described in the previous section and the time events which are inserted into the data stream every millisecond. The wobble geometry is shown in Fig. 3. D1 and D2 are the coincident detectors for a certain event. Line *ab* is the projection normal for the line of response (LOR) of

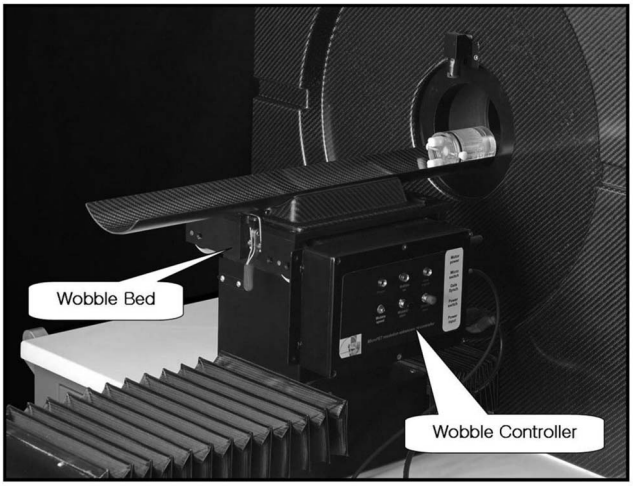

FIG. 2. A wobble system has been installed underneath the animal bed of MicroPET R4 scanner

the projection angle θ. At a certain point during a scan, δ defines the current wobble displacement for a wobble radius r. It is given by

$$\delta = r \cdot \cos(\omega - \theta), \tag{2}$$

where ω is the wobble angle which can be calculated from the time of the last wobble-origin pulse and the duration of the previous wobble cycle. The wobble angle is given by

$$\omega = 2\pi \cdot \frac{t - \omega_1}{\omega_1 - \omega_2}, \tag{3}$$

where t is the time of the coincidence event, ω_1 is the nearest previous gate time, and ω_2 is the next gate time.

Dwell time, that is the time spent in each wobble cycle during which counts contribute to each wobble bin, must be corrected for when using the wobble motion. The dwell is proportional to the arc length along the circumference of the wobble circle assigned to each wobble bin, since the bed

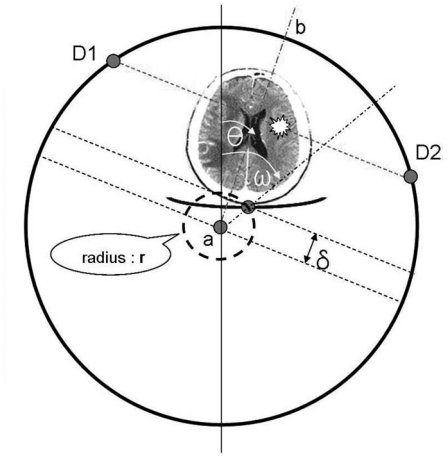

FIG. 3. Wobble displacement may be decided from the wobble radius r, the wobble angle ω, and the projection angle θ.

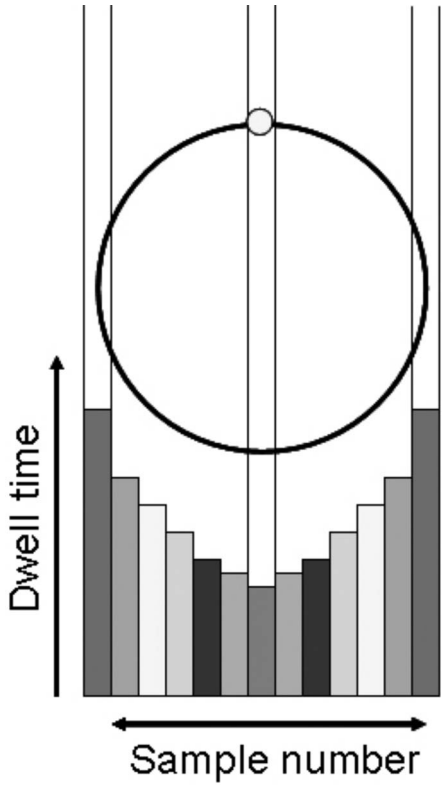

FIG. 4. The dwell time during the wobble cycle is the time during which the events contribute to each sample in the projection. It must be corrected for during the histogramming.

spends different duration in each bin on the projection. The dwell effect is demonstrated in Fig. 4. To account for this, we need to add a weighting factor that is inversely proportional to the dwell time instead of adding a constant value to the sinogram.

It is necessary to apply both the arc correction and normalization into the histogramming program before performing the rebinning. The arc correction maps the lines of response from each detector pair onto a uniformly sampled projection by interpolation. This is due to the fact what while LORs become closer as the radial offset increases, the wobble radius remains constant. This prevents the normal arc correction from being applied to the data after rebinning. The crystals within each block are not the same distance apart as those which are nearest neighbors in adjacent blocks. The gaps between blocks appear in different places in different projections. We performed Monte Carlo simulations with PETSIM (Ref. 14) to find the precise distance of each LOR from the center of the projection. A look-up table of LOR positions was generated and it is used to find the accurate distance of each LOR. Since there are eight crystals in a column per block, there are 16 offset tables required. Similarly, normalization has to be applied before the wobble correction because the corresponding detector pairs may be changed by the wobble correction.

The new histogramming program uses the full three-dimensional (3D) data set to generate wobble corrected sinograms. It arranges the 3D sinograms in the same order as the

standard sinogram set and generates output in the same format as the standard one. The new sinogram can thus be opened with any of the MicroPET reconstruction programs as well as "ASIPro," the image analysis tool for MicroPET scanners.[15] All of the reconstruction programs used with the MicroPET work with the wobbled sinograms but the arc correction, normalization, and smoothing features are disabled since they are already applied during the histogramming.

The wobbled sinogram contains many more elements than the standard sinogram, so that the number of counts per element is reduced. To account for this, the reconstruction filter must be adjusted to boost frequencies that can be captured by the detector-pairs' response, while suppressing those which contain only noise. A Wiener filter is applied to the wobbled sinogram prior to image reconstruction in order to optimize the trade-off between image noise and spatial resolution. The applied Wiener filter is shown in Fig. 5.

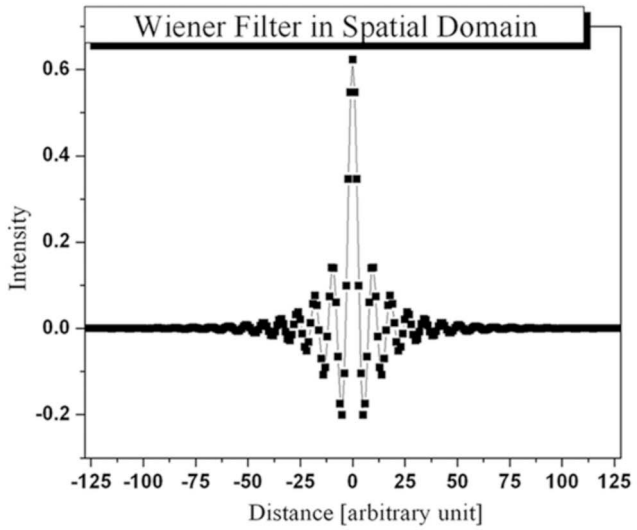

(a)

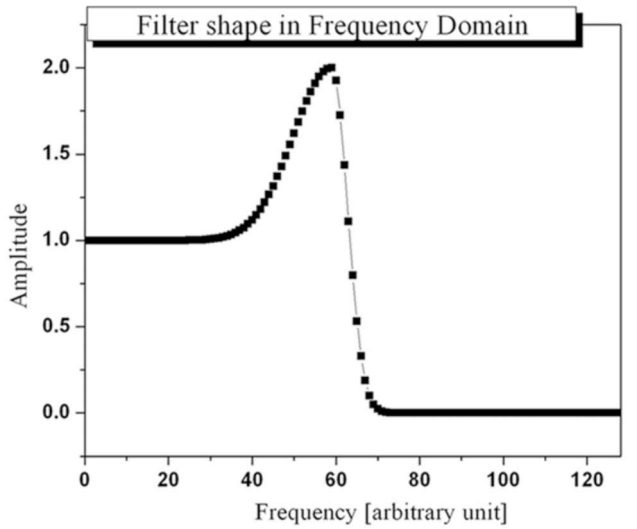

(b)

FIG. 5. A Wiener filter, which is the mean-squared error-optimal stationary linear filter for images degraded by additive noise and blurring, is used to refine data processing. Wiener filter shapes in spatial domain (a) and in frequency domain (b) are plotted.

II.C. Experimental methods

II.C.1. Optimal wobble radius for MicroPET R4

To determine the optimal wobble radius for the MicroPET R4 scanner, the overall shape and FWHM of profiles in the sinograms from a series of scans of a ^{22}Na point source were compared. The activity of the source was 56.8 μCi. The ^{22}Na point source was scanned with all available wobble radii for 10 min per scan. The FWHM of the source profile in each sinogram was measured. This source has a "scatterless" configuration in which the activity is applied as a 3 mm spot centered between two laminated 0.9 mg/cm^2 Mylar foils sandwiched between two removable aluminum disks. The source was acquired from Isotope Products Laboratories, an Eckert & Ziegler Co.

II.C.2. Measurement of the peak-to-valley ratio of two point sources

The ^{22}Na source was scanned for 5 min near the CFOV and then was moved in 0.50 mm steps away from the CFOV until it reached a distance of 3.00 mm away from the center. When it was scanned at positions farther than 3.00 mm from the CFOV, the step size was decreased to 0.20 mm. MicroPET ASIPro VM has a function, so called "add" in "image calculator" of its toolbox, which makes one overlapped image from two independent images. One image with two adjacent and exactly identical point sources can be achieved by using this add function. The average values of the two peaks were used for peak-to-valley ratio calculation.

II.C.3. Scans performed on a resolution phantom

The Data Spectrum Micro ECT phantom was filled with room temperature water and ^{18}F-FDG. The phantom consists of a cylinder with an internal diameter of 4.4 cm and a rod insert with six sectors of fillable rods of diameters 1.2, 1.6, 2.4, 3.2, 4.0, and 4.8 mm. The center-to-center distance of the rods is equal to twice the diameter of the rods. This phantom was scanned without wobbling motion for 1 h and then scanned again with wobbling motion. The scan time for the wobbling acquisition was increased to account for the decay of the ^{18}F activity. This was accomplished by acquiring data for the second scan until a similar number of prompt counts were acquired as in the first scan (305 million). The activity was 670 μCi at the beginning of the first scan and the initial activity at the start of the wobbled scan was 310 μCi. The timing window was set at 6 ns and lower and upper level discriminator values of 350 and 750 keV, respectively, were used.

Single slice rebinning was used to generate the sinogram for the nonwobbled scan using a span of 3 and ring difference of 1. The image was reconstructed using the two-dimensional (2D)-filtered backprojection (FBP) algorithm. A ramp filter was chosen with a Nyquist cutoff value of 0.5 for the nonwobbled scan and 0.1666 for the wobbled scan. The

Nyquist cutoff value of the wobbled scan was one-third that of the nonwobbled scan since the rebinning factor of the wobbled correction was set at 3. In order to investigate the effect of wobbling on the spatial resolution, no additional smoothing filter was applied for this phantom image since this would degrade the spatial resolution of the image.

II.C.4. FDG scans performed on rat brain

An 833 g Sprague–Dawley rat was scanned with and without wobbling motion. The nonwobbled scan was performed first, 40 min after the injection of 501 μCi ^{18}F-FDG. The activity was 389 μCi at the beginning of the scan and data were acquired for 20 min. The initial activity at the start of the wobbled scan was 318 μCi and the scan was performed for 30 min. The nonwobbled scan was histogrammed into a 3D sinogram using a span of 3 and ring difference of 31. The wobbled scan was histogrammed into a 3D sinogram with the same span and ring difference by our own histogramming program which can handle the wobble effect. The images were reconstructed using Fourier rebinning followed by 2D-FBP with a ramp filter.

II.C.5. Comparison of reconstruction times with various reconstruction techniques

One static nonwobbled FDG image was reconstructed with three reconstruction methods offered by the manufacturer and these were compared with the wobbled scan reconstructed with the 2D-FBP technique. The standard software provides FBP, 2D, and 3D versions of ordered subsets expectation maximum (OSEM), and the maximum *a priori* (MAP) algorithm which incorporates knowledge about the scanner's system matrix into the reconstruction process. We use 2D-FBP after applying all the corrections and optimizations during histogramming for the wobbled scan.

III. RESULTS

III.A. Optimal wobble radius for MicroPET R4

The FWHMs of the profiles were calculated from ten different projection angles of all possible wobble radii. Each profile was compared with other profiles from the same projection angle of other wobble radii. The average of the FWHMs versus wobble radii is shown with standard errors in Fig. 6. When the wobble radius is set to be 1.50 mm, the source profiles have the minimum FWHMs. This value is slightly larger than half of the 2.426 mm crystal pitch used in the MicroPET R4 scanner.

III.B. Peak-to-valley ratio of two point sources

The measurement of the peak-to-valley ratio versus source separation is shown in Fig. 7. The sources are not resolved at all for both nonwobbled and wobbled acquisitions when the separation is less than 2.50 mm. The difference between the peak-to-valley ratios for the wobbled and nonwobbled acquisitions gradually grows as the source separation increases beyond 2.50 mm. The peak-to-valley ratio is improved from 1.75 to 2.26 by applying wobbling motion when the separation is equal to 4.0 mm.

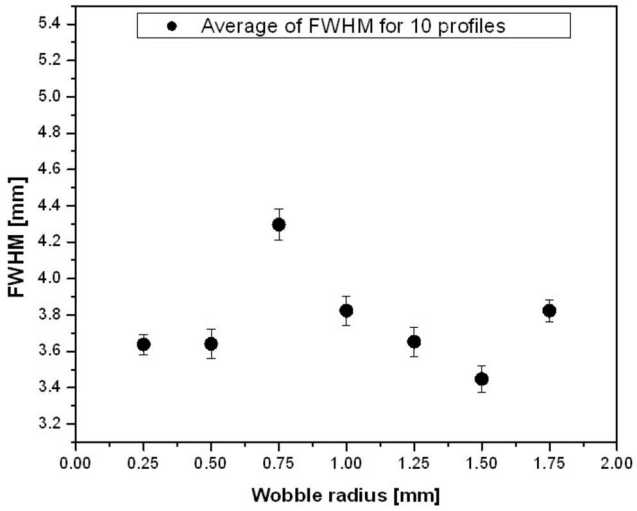

FIG. 6. The average of the FWHMs are calculated from the FWHMs from ten different positions on sinograms for each wobble radius.

III.C. Resolution phantom

Figure 8 shows a slice of the transverse image of the phantom and its profile with and without the wobble effect. The upper profile (a) and image (b) are for the nonwobble case and the bottom profile (c) and image (d) are for the wobbled scan. Without wobble motion, rod diameters of 1.2 and 1.6 mm in the phantom are hardly distinguishable in the image (b). In comparison, most rods of diameter 1.6 mm can be recognized in the wobbled image (d) of Fig. 8. The profiles (a) and (c) were generated from the selected area on the images (b) and (d), respectively.

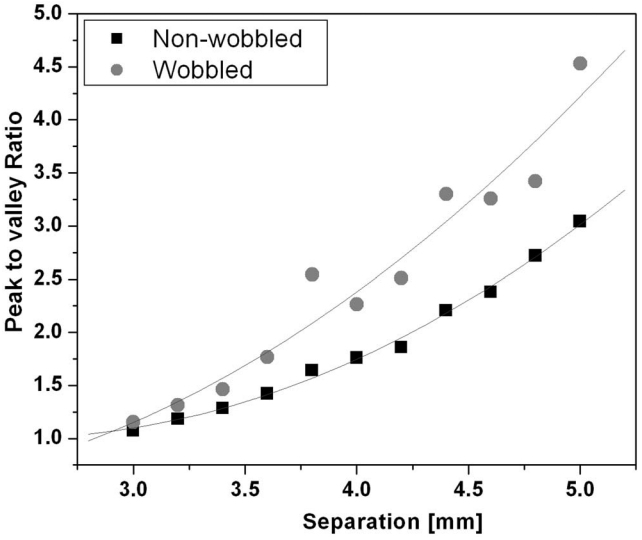

FIG. 7. The peak-to-valley ratio vs separation of two point sources.

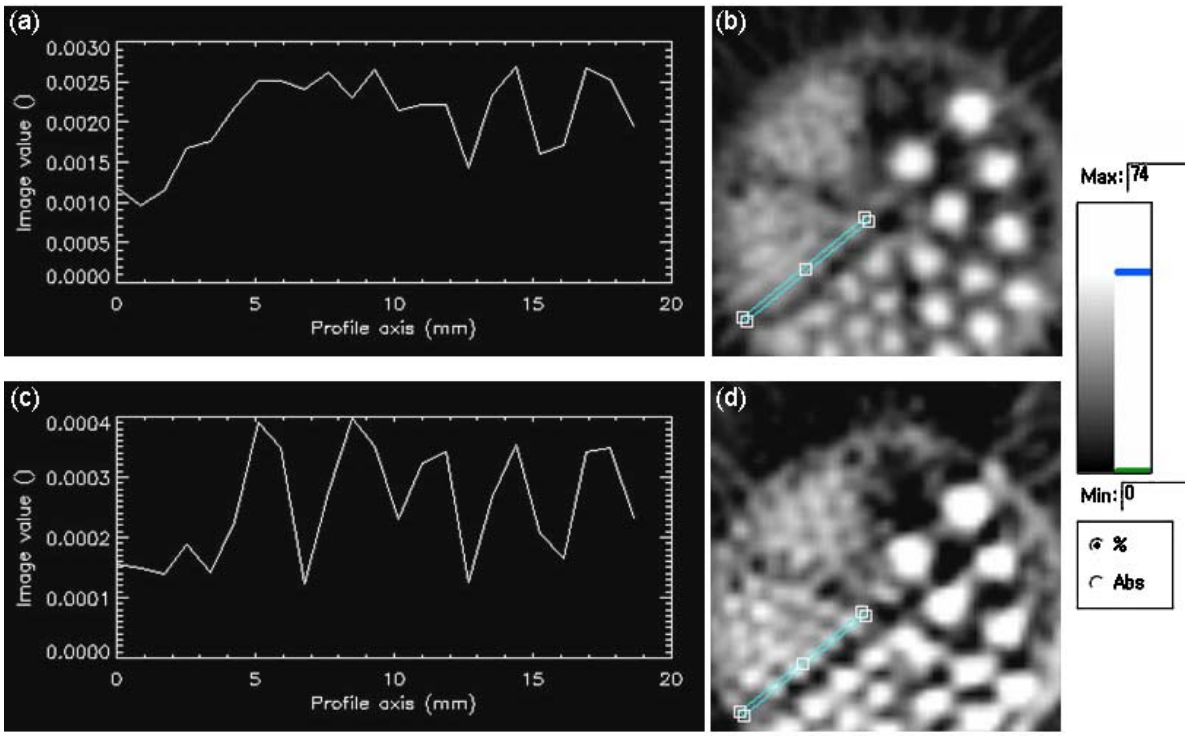

FIG. 8. A slice (x:64, y:64, z:53) of the phantom image (b), (d) and the profile (a), (c) from the selected area on the image. The upper profile (a) and image (b) correspond to data acquired without wobble motion. The bottom profile (c) and the image (d) are from the data acquired with wobble motion. Six sectors of solid rods of diameters are 1.2, 1.6, 2.4, 3.2, 4.0, and 4.8 mm and the profiles are compared at the area of 1.6 mm rods.

III.D. FDG rat brain study

Figure 9 shows the transverse images of a rat brain with and without wobbling motion. The striatum can be visualized in the wobbled image while it is not visible on the image from the nonwobbled scan. The carotid arteries, two round dots at the bottom of image, are more distinctly seen for the case of the wobbled acquisition. Throughout all transverse slices, the image from the wobbled scan shows better resolution than the image from the nonwobbled scan, with improvements similar to Fig. 9.

III.E. Comparison of reconstruction times with various reconstruction techniques

The times for various reconstruction techniques were measured for a single frame study on a 2.16 GHz single processor computer with 2 Gbyte RAM. The times do not include the time for histogramming, but this time is approximately the same when including all the wobble corrections as when using the conventional technique. The reconstruction time of the wobbled scan is three times longer than the time of 2D-FBP reconstruction of a normal scan since the number of bins is increased by factor of 3. The MAP reconstruction times are two orders of magnitude longer. Table I shows the reconstruction time for various reconstruction algorithms for the MicroPET R4 scanner. The reconstruction times for various algorithms with/without wobbling are measured on a 2.16 GHz processor and 2 Gbyte RAM computer. Figure 10 shows rat brain images reconstructed by the 2D-FBP and MAP algorithm without wobble motion as well the 2D-FBP algorithm with wobble motion.

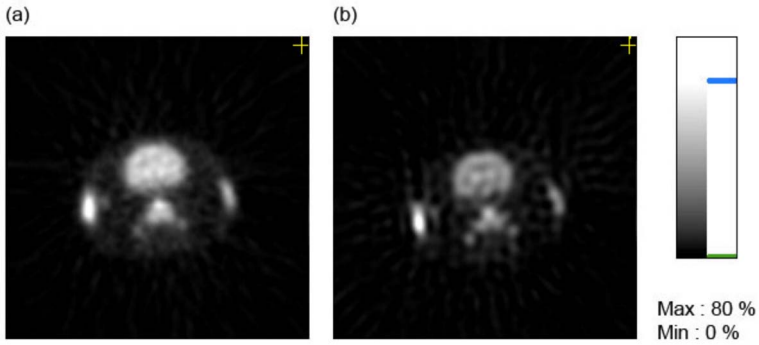

FIG. 9. A transverse slice (z=26) from a rat brain image with and without wobble effect. (a) shows the image from the stationary scan and (b) shows the image with wobbling motion.

TABLE I. The reconstruction time for various algorithms on a 2.16 GHz processor, 2 Gbyte RAM computer.

Algorithm	MAP	OSEM3D/MAP	OSEM2D	2D-FBP	Wobble scan new histogramming program (rebinning factor 3) Wiener filter, 2D-FBP
Reconstruction time (s)	1350	1700	54	5	16

IV. DISCUSSION

In this work, the greatest improvement in spatial resolution for the MicroPET R4 was obtained when a wobble radius of 1.50 mm was used. Of all the wobble radii examined, this choice most uniformly samples the object at the CFOV throughout all of the projection angles during the wobble cycle and at the same time minimizes the overlapped area between two adjacent crystals. If the wobble radius is smaller than 1.50 mm, the wobble motion may not span the full intercrystal pitch properly. In contrast, if it is larger than 1.50 mm, a larger overlapping area between two adjacent detectors may make the relative concentration of data in adjacent bins unacceptably large. This concept of "spanning" the intercrystal pitch is shown in Fig. 11. Therefore, the optimal wobble radius of the MicroPET R4 system was found to be 1.50 mm when the magnification and rebinning factors are set to be 3. The sampling density is higher near the ends of the projections due to the ring structure of detector system while the wobble radius is constant. This is the reason why the optimal wobble radius is not obvious and needed to be determined empirically.

The peak-to-valley ratio of two separated point sources shows an improved spatial resolution when the wobble motion is applied. The peak-to-valley ratio was improved from 1.75 to 2.26 when the sources are separated by 4.00 mm. This distance approximately corresponds to the separation of the striatum of an adult rat. This suggests that one would get a finer image of the rat striatum by incorporating a wobbling bed motion. This improvement was demonstrated from the visual inspection of the rat image.

Visual inspection of the resolution phantom images also showed that the wobbling mechanism improved the spatial resolution of MicroPET R4 scanner. The image from the wobbled scan shows improved contrast when compared to the nonwobbled scan. In addition, the improvement of the spatial resolution of images is clearly shown on the profiles for each scan. Several peaks can be distinguished in the profile with the wobble motion, while these peaks are hardly seen in the profile generated without wobble motion.

Finally, images of a rat confirm that wobbling motion may be very helpful in neuroimaging research studies of small animals. As shown in Fig. 9, the striatum becomes more visible in the image acquired using the wobble motion. Other structures, like the carotid arteries, also stand out more distinctly in the image from the wobbled scan. It took 16 s to reconstruct the image from the wobbled scan using the FBP algorithm (c), while image reconstruction using the MAP algorithm took more than 23 min (b). Although it took a much shorter time to be reconstructed, the FBP image from the wobbled scan showed a greater amount of anatomical detail and more easily distinguishable striatum.

It worth noting that the wobble acquisition and processing method presented in this article provides a fast reconstruction algorithm compared with those like "MAP" which incorporate a model of the scanner's system matrix. One could consider that combination of the increased spatial sampling by wobbling motion, interpolation of the detector pair positions onto a non uniform grid based on Monte Carlo simulation and optimization of the filter to suppress frequencies which are beyond the normal Nyquist frequency as being equivalent to the "system matrix" used to optimize MAP reconstruction, but without the penalty of long reconstruction times.

V. CONCLUSION

The undersampling of the image space in a conventional animal PET scanner can be overcome by adding a bed wobbling mechanism without applying any other significant changes to the scanner. We have designed and built a simple wobble mechanism for improving the sampling density. The wobble mechanism applies a continuous eccentric circular movement to the scanner's animal bed in the gantry during a scan. The wobble controller allows adjustment of wobble speed and produces gating signals when the bed passes

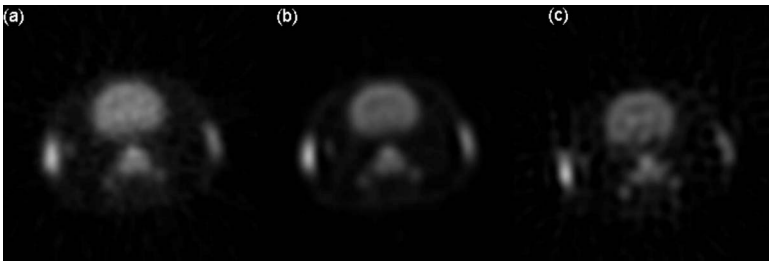

FIG. 10. Three rat brain images reconstructed by FBP (without wobble motion), MAP (without wobble motion), and FBP (with wobble motion) are shown in (a), (b), and (c), respectively. The striatum is more distinguishable in (c) than (b), although reconstruction time for (c) was much faster than (b).

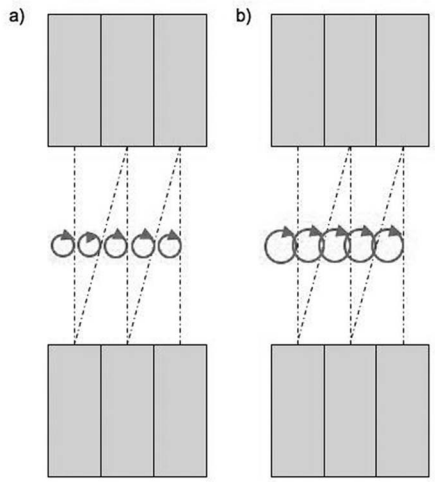

FIG. 11. Wobble radius has to be larger than the half of the crystal pitch, otherwise wobbling motion cannot span whole FOV. (a) shows the case when the wobble radius is smaller than the half of the crystal pitch and (b) shows the case when the wobble radius is larger than the half of the crystal pitch.

through the top position of each circle. A new histogramming program which histograms the list-mode data of the MicroPET R4 scanner was written and tested. All corrections discussed in this article were added to the histogramming program and are able to be used on full 3D sinogram data sets. The accurate positions of all possible LORs were simulated with PETSIM and the simulated data were used to make a look-up table which is used to correct for nonuniformities of the raw sampling density.

The optimal wobble radius was empirically determined to be 1.50 mm for MicroPET R4 scanner when the magnification and rebinning factor was set to be 3. The peak-to-valley ratio showed that the spatial resolution was improved by wobbling the bed. This result was confirmed by visual inspection of the images of a resolution phantom and images of a rat brain. The striatum and arteries were more clearly distinguished on images acquired using the wobble motion. The results presented in this article show that the continuous wobble motion during the scan increases the sampling rate and this leads to an improvement in the spatial resolution of the scanner.

ACKNOWLEDGMENTS

We gratefully acknowledge Dr. Pedro Rosa-Neto and Antonio Aliaga for their help with the animal studies. This work was supported by a grant from the Natural Sciences and Engineering Research Council of Canada OPG:0033672 to C. J. T. at the Montreal Neurological Institute.

[a]Author to whom correspondence should be addressed. Present address: Brain Research Centre, University of British Columbia, 2211 Wesbrook Mall, Vancouver, British Columbia V6T 2B5, Canada. Telephone: +1 (604) 822-7149; Fax: +1 (604) 822-7299. Electronic mail: joon@physics.ubc.ca

[1]C. Knoess *et al.*, "Performance evaluation of the microPET R4 scanner for rodents," Eur. J. Nucl. Med. Mol. Imaging **30**, 737–747 (2003).
[2]W. W. Moses and S. E. Derenzo, "Empirical observation of resolution degradation in position emission tomographs utilizing block detectors," J. Nucl. Med. **34**, 101P (1993).
[3]S. E. Derenzo, W. W. Moses, R. H. Huesman, and T. F. Budinger, *Quantification of Brain Function* (Elsevier Science, Amsterdam, 1993), pp. 25–37.
[4]R. Laforest, D. Longford, S. Siegel, D. F. Newport, and J. Yap, "Performance evaluation of the microPET Foces-F120," IEEE Trans. Nucl. Sci. **54**, 42–49 (2007).
[5]N. Tomic, C. J. Thompson, and M. Casey, "Investigation of the 'Block Effect' on spatial resolution in PET detectors," IEEE Trans. Nucl. Sci. **52**, 599–605 (2005).
[6]Based on data presented at the conference on High Resolution Imaging in Small Animals with PET MR and Other Modalities, Amsterdam, The Netherlands, 1999.
[7]C. J. Thompson, S. St. James, and N. Tomic, "Under-sampling in PET scanners as a source of image blurring," Nucl. Instrum. Methods Phys. Res. A **545**, 436–445 (2005).
[8]M. M. ter-Pogossian, M. Yamamoto, and D. Ficke, "Performance study of pett vi, a positron computed tomograph with 288 cesium iodide detectors," IEEE Trans. Nucl. Sci. **29**, 529 (1982).
[9]C. J. Thompson and A. Dauger, "A real time data rebinning in PET to obtain uniformly sampled projections," IEEE Trans. Nucl. Sci. **32**, 811–817 (1985).
[10]A. C. Evans *et al.* "Performance evaluation of the PC2048, a new 15-slice encoded crystal PET scanner for neurological studies," IEEE Trans. Med. Imaging **10**, 90–98 (1991).
[11]A. Chatziioannou *et al.* "Techniques to improved the spatial sampling or MicroPET—A high resolution animal PET tomograph," IEEE Trans. Nucl. Sci. **47**, 422–472 (2000).
[12]C. J. Thompson, A. Dagher, E. Meyer, and A. C. Evans, "Imaging performance of a dynamic PET: Positome IIIp," IEEE Trans. Med. Imaging **MI-5**, 183–198 (1986).
[13]J. Y. Suk, "Improving the spatial resolution of the MicroPET R4 scanner by wobbling the bed," M.Sc. thesis, McGill University, Montreal, Quebec, Canada, 2007.
[14]C. J. Thompson, J. J. Moreno-Cantu, and Y. Picard, "PETSIM: Monte Carlo simulation of all sensitivity and resolution parameters of cylindrical positron imaging systems," Phys. Med. Biol. **37**, 731–749 (1992).
[15]Siemens Preclinical Solutions, Manual of ASIPro VM™ version 6.2.5, 2005.